

Preparation of SnO₂/TiO₂/C composite fibres and their use as binder-free anodes for lithium-ion batteries

GABRIEL GONZALEZ¹, DAVID SANCHEZ¹, DANIEL RAMIREZ², JASON C MYERS³, TIMOTHY P LODGE⁴, JASON PARSONS² and MATAZ ALCOUTLABI^{1,*}

- ¹Department of Mechanical Engineering, University of Texas, Rio Grande Valley, Edinburg 78539, USA
- ²Department of Chemistry, University of Texas, Rio Grande Valley, Brownsville 78521, USA
- ³College of Science and Engineering, 55 Shepherd Labs, University of Minnesota, Minneapolis 55455-0431, USA
- ⁴Department of Chemical Engineering and Materials Science and Department of Chemistry, University of Minnesota, Minneapolis 55455-0431, USA
- *Author for correspondence (mataz.alcoutlabi@utrgv.edu)

MS received 23 August 2022; accepted 14 November 2022

Abstract. Tin dioxide/titanium dioxide/flexible and carbon fibres ((SnO₂/TiO₂)/FPCFs) were fabricated via centrifugal spinning (CS) of precursor solutions and used as binder-free anode materials in lithium-ion batteries (LIBs). The SnO₂/TiO₂/FPCFs were prepared by CS of tin (II) 2-ethylhexanoate/titanium (IV) butoxide/polyvinylpyrrolidone, followed by calcination at 700°C to yield SnO₂/TiO₂ short fibres. The as-obtained fibres were crushed and mixed in ethanol to form a SnO₂/TiO₂/ethanol solution. Polyacrylonitrile/polymethyl methacrylate (PAN/PMMA) fibrous mats were also prepared via CS of PAN/PMMA/DMF solutions and were coated with the SnO₂/TiO₂/ethanol solution and then heat-treated to yield SnO₂/TiO₂/FPCFs. The structure and morphology of the composite fibres were investigated by scanning electron microscope, energy dispersive X-ray spectrometer), transmission electron microscopy, X-ray diffraction, X-ray photoelectron spectroscopy and thermogravimetric analysis. When used as binder-free anodes for LIBs, the (3:2) (SnO₂:TiO₂)/FPCFs exhibited a high reversible capacity of 890 mAh g⁻¹ and demonstrated an outstanding columbic efficiency of 98% after 100 charge/discharge cycles at a current density of 100 mAh g⁻¹ and good rate capability. For comparison, the electrochemical results of (SnO₂)/FPCFs and (SnO₂/TiO₂)/FPCFs with 1:1 (SnO₂:TiO₂) ratio are also reported.

Keywords. SnO₂; lithium-ion battery; centrifugal spinning; composite fibres; anode; TiO₂.

1. Introduction

The high demand for energy has led to excessive use of fossil fuel, resulting in many environmental issues including substantial CO₂ emissions. Lithium-ion batteries (LIBs) are considered as an alternative energy source to fossil fuels for use in electric vehicles (EVs), electronics, and portable devices owing to their compact size, high energy density and high specific storage capacity [1-6]. Although they have proven to outperform other sources of power such as wind and solar energy, LIBs have not yet reached their optimal potential. Currently, the most common anode material used in LIBs is graphite, but it can only deliver a specific capacity of 372 mAh g⁻¹ [7-9]. Another limiting factor of graphite is the formation of surface dendrites during rapid charging. This phenomenon leads to a low Li⁺ diffusivity that can compromise the electrochemical performance of the battery [10-12].

In the search for alternative anode materials, metals such as Sn, Ti, and (iron) Fe as well as their respective oxides have been widely investigated due to their distinct chemical and physical characteristics and high capacities ranging from 500 to 1000 mAh g^{-1} [13–16]. More recently, nano/ micro-structured metal oxides have been synthesized through various methods and have exhibited improved electrochemical performance when compared to their bulk counterparts. In addition, metal oxides are of interest due to their environmental friendliness, abundance and low cost [17,18]. Sn and SnO₂ have been widely investigated as alternative anode materials due to their high theoretical capacity of 993 and \sim 782 mAh g⁻¹, respectively [19–22]. Despite its high capacity, Sn suffers from a high volume expansion during the alloying/dealloying process with lithium, which can result in anode cracking and capacity fading [23–25]. Similarly, SnO₂ is brittle and suffers from huge volume expansion after prolonged charge/discharge cycles, which can lead to pulverization and poor cycling performance of the anode. To improve the electrochemical performance and reduce the volume change of Sn and SnO₂ anodes, the design of new nano/micro-structures in combination with other materials such as TiO2 and carbon have been recently investigated [19–21,24,26–28]. TiO₂ has been

Published online: 27 March 2023

of interest in LIB research for its excellent rate performance, low volume change upon cycling, and good capacity retention over long periods of time. When combined with Sn and SnO₂, Sn/TiO₂ or SnO₂/TiO₂ composite anodes can maintain high capacity and low volume change after prolonged charge/discharge cycles [19, 29–34].

Sn/TiO₂ and SnO₂/TiO₂ composites have shown promising results when compared to pristine Sn and SnO₂, but they still suffer from pulverization after prolonged charge/discharge cycles. To further improve the electrochemical performance of Sn and SnO₂, various carbon coating methods have been explored to reduce the large volume change and stresses developed during charge/discharge cycles [9,15,19,25,30,35–39]. Due to their high porosity and high surface area, carbon fibres (CFs) have been widely used as stress buffer matrices for metal and metal oxide-based anodes. Compared to their bulk counterparts, CFs provide larger numbers of reaction cites for Li⁺ intercalation that can result in higher anode capacity [40–42].

Electrospinning has been amongst the most used methods to prepare various composite carbon fibres, such as porous, hollow and multichannel structures. Electrospinning allows facile fibre production and the synthesis of various metal oxide/carbon fibres with distinct nanostructures for LIB and other applications [43–45]. For example, Mou et al [46] used electrospinning to prepare encapsulated SnO₂/TiO₂ particles in carbon nanofibres. Li et al [47] synthesized porous carbon nanofibres containing Sn/Ti nanoparticles through electrospinning and subsequent heat treatment. When used as an anode material in LIBs, the Sn/Ti/C composite fibres delivered a capacity of 557 mAh g⁻¹ at 100 mA g⁻¹, higher than graphite [47]. Additionally, the assynthesized composite fibres demonstrated a capacity retention of 98.7% after 100 cycles at a current density of 50 mA g⁻¹, which was attributed to the buffering effect of the flexible carbon-fibre matrix [30,47-50]. Although promising results have been reported using electrospinning, the required high applied voltage as well as low production rates limit the use of this technology [45,51].

More recently, centrifugal spinning (CS) has been explored as an alternate method to produce carbon composite fibres. CS relies solely on centrifugal forces and high rotational speeds to yield large quantities of fibres [40,51-53]. Currently, centrifugally spun composite fibres have been used as binder-free anodes in LIB and sodium-ion batteries (SIBs) and have exhibited good electrochemical performance [54–56]. Agubra et al [57] synthesized Sn/C composite fibres via CS of Sn/poly(acrylonitrile) (PAN) precursor solutions followed by subsequent heat treatment. When applied as binder-free anodes in Li-ion half-cells, the Sn/C composite fibres delivered a high reversible capacity of 724 mAh g⁻¹ after 50 cycles at a current density of 100 mA g⁻¹, which was attributed to the flexible and amorphous structure of the CFs [57]. Work reported on centrifugally spun SnO₂/C composite-fibre anode for SIBs showed that the composite anode delivered a capacity of 158 mAh g⁻¹ after 100 cycles at 640 mA g⁻¹ and exhibited good rate performance. Although improved electrochemical results have been obtained by CS, such technology still faces some challenges. For example, high loadings of active material (e.g., Sn, Si or Sb nanoparticles) in the precursor solution and uniform distribution of active material within the fibres can be difficult to achieve due to high viscosity and particle agglomeration. Although solutions with high viscosity are preferred for CS compared to electrospinning, the addition of active material to the polymer solution can greatly increase the solution viscosity and can negatively affect the formation and the production rate of the composite fibres [54,58,59]. To address these issues, different coating methods have been explored to load the active material (e.g., nanoparticles or short fibres) onto centrifugally spun precursor fibres with the aim to improve the anode performance [60,61].

In the present work, ternary (SnO₂/TiO₂)/FPCFs composites were prepared by CS of precursor solutions and subsequent heat treatment. The characterization of the composite fibres was studied by scanning electron microscope (SEM), energy dispersive X-ray spectrometer (EDS), transmission electron microscopy (TEM), X-ray diffraction (XRD), X-ray photoelectron spectroscopy (XPS) and thermogravimetric analysis (TGA). Moreover, when used as binder-free anodes in LIBs, the composite fibres with 3:2 (SnO₂:TiO₂) ratio demonstrated outstanding electrochemical results. For comparison, the electrochemical results of SnO₂/FPCFs and SnO₂/TiO₂/FPCFs with 1:1 (SnO₂:TiO₂) ratio were also investigated.

2. Experimental

2.1 Materials and fibre preparation

Poly(methyl methacrylate) ($M \approx 20,000$), poly(acrylonitrile) (PAN) ($M \approx 150,000$), poly(vinylpyrrolidone) (PVP) ($M \approx 1,300,000$), tin (II) 2-ethylhexanoate, titanium (IV) butoxide, N,N-dimethyl formamide (DMF), absolute ethanol (200 proof), conductive carbon black, ethylene carbonate and dimethyl carbonate were all purchased from Sigma-Aldrich (USA) and used as received. Lithium salt (LiPF₆) and commercial lithium foil were purchased from MTI (USA). Whatman glass microfibres were purchased from GE Healthcare and used as separators in Li⁺ half-cells. Ceramic and ceramic/carbon composite fibres were prepared by CS using a FiberLab L1000 (FibeRio) at various spinneret rotational speeds.

2.2 Characterization

The surface and elemental composition of the as-prepared composite fibres were studied with a scanning electron microscope (SEM) equipped with a Sigma VP Carl Zeiss instrument as well as an energy dispersive X-ray

spectrometer (EDS) from EDAX (Mahwah, NJ, USA). The thermal degradation of the precursor fibres was investigated by TGA in air over a temperature range between 50 and 700°C at a heating rate of 5°C min⁻¹. XRD and XPS analyses were performed to identify the crystal structure/crystal phase of the oxidized fibres as well as to study the surface chemistry of the fibres, respectively. The XRD patterns were obtained using a Rigaku Bruker D2 X-ray Diffractometer equipped with a Co source (K_{α} $\lambda = 1.789$ Å), while the XPS spectra were collected using a Thermoscientific K-α instrument equipped with monochromatized Al Kα radiation (1486.7 eV). TEM images and selected area electron diffraction images were captured using a FEI G2 F30 microscope with a working voltage of 300 kV. The high-angle annular dark field scanning TEM and EDS maps were acquired with a FEI G2 Titan 60-300 probe corrected microscope equipped with a Super-X EDS system. The Titan was used at 200 kV with a convergence angle and a high-angle annular dark field inner collection semi-angle of 24 and 58.6 mrad, respectively.

2.3 Anode preparation

2.3a Preparation of anodes from SnO₂ and SnO₂/TiO₂ composite fibres: The SnO₂ and SnO₂/TiO₂ ceramic fibres were prepared by oxidation of the centrifugally spun precursor fibres. First, 3 g of PVP were dissolved in 17 g of ethanol, followed by magnetic stirring for 12 h at temperature. Then, 1.5 g of 2-ethylhexanoate and Ti(IV) butoxide, in 100:0, 1:1 and 3:2 weight ratios were added to the PVP/ethanol solution followed by an additional 12 h of magnetic stirring to achieve homogeneity. A syringe was used to load the solution onto the CS equipment. The solution was spun at 9000 rpm and a relative humidity of 55% to yield SnO₂/PVP and SnO₂/TiO₂/PVP precursor fibres. The SnO₂ and SnO₂/TiO₂ short fibres were obtained by calcination of the as-prepared precursor fibres at 700°C in air. To prepare the anodes, the as-prepared short fibres were manually crushed with a mortar and pestle to reduce agglomeration. Then, a slurry containing short fibres, PAN and carbon black were mixed in 1 g of DMF with 80:10:10 (short fibres: PAN: carbon black) ratio. The slurry was then sonicated for 30 min and magnetically stirred for 12 h to achieve homogeneity. The as-prepared slurry was coated onto a copper foil with a thickness of 25 microns and dried under vacuum at 60°C for 24 h. Finally, the slurry was heat-treated in a tube furnace filled with argon at 450°C for 5 h at a heating rate of 2°C min⁻¹ (i.e., heating from 25 to 450°C). The as-obtained heat-treated slurry was cut into 0.5" diameter discs and utilized as anode materials for Li-ion half-cells.

2.3b Preparation of anodes from SnO₂ and SnO₂/TiO₂ flexible and carbon fibres: A quantity of 1.92 g of PAN was dissolved in 17.6 g of DMF by magnetically stirring for 12 h to prepare a homogeneous solution. Then, 0.48 g of PMMA was added while the solution was left to stir for an additional 12 h at 60°C. The PAN/PMMA solution was then loaded into a syringe and fed into a spinneret to prepare centrifugally spun PAN/PMMA pristine 8500-9000 rpm with a relative humidity of 55-60%. The obtained precursor fibres were then dried under vacuum overnight at 60°C to evaporate any remaining solvent. Prior to preparing the coating solution, TGA was conducted on the PAN/PMMA fibres to determine the carbon yield after carbonization at 700°C [62]. The coating solution was then prepared by mixing 50 wt% of short microfibres, with (3:2) (SnO₂/TiO₂) weight ratio in ethanol followed by sonication for 1 h and magnetic stirring for 24 h. The coating solution was then loaded into a syringe and coated onto the pristine PAN/PMMA fibres. The coated fibres were then dried under vacuum at 60°C for 24 h. To obtain flexible ternary SnO₂/ TiO₂/C composite fibres, the metal-oxide-coated precursor fibres were stabilized in air at 280°C for 6 h (heating rate of 3°C min⁻¹) and carbonized at 700°C for 3 h in an argonfilled tube furnace (heating rate of 5°C min⁻¹). To prepare pure FPCFs, the same heat treatment was applied to PAN/ PMMA pristine fibres. The obtained carbon fibres were cut into discs with 0.5 in diameter and used as binder-free anodes in LIBs. The total mass of the SnO₂/TiO₂/C anode was about 3.32 mg and the mass of the SnO₂/TiO₂ active material in the electrode was about 1.73 mg, while the mass of carbon in the electrode was about 1.49 mg.

2.4 Electrochemical evaluation

The as-prepared 0.5" SnO₂ and SnO₂/TiO₂ ceramic/carbon fibre anodes were placed in an argon-filled glove box (O₂, H₂O concentrations < 0.5 ppm MBRAUN, USA). Li⁺ halfcells (CR 2032 PHD Energy Inc.) with Li-metal as the counter electrode and glass microfibres as the separator were used. The electrolyte was prepared from 1 M LiPF₆ in ethylene carbonate/dimethyl carbonate (1:1 v/v) and used without any further additives. Cyclic voltammetry experiments were performed at a scan rate of 0.1 mV s⁻¹ over a voltage range between 0.05 and 3.0 V (Biologic Science Instruments, France). Electrochemical impedance spectroscopy (EIS) experiments were conducted on Li-ion halfcells in the frequency range between 0.1 and 100,000 Hz using Metrohm Autolab (PGSTAT 128 N, Metrohm). The electrochemical performance of the anodes was evaluated by galvanostatic charge-discharge experiments using a LANHE battery testing system (CT2001A) with an applied current density of 100 mA g⁻¹ over 70 cycles over the potential range 0.05-3.0 V. The rate capability of the composite-fibre anodes was studied using Arbin battery

tester with a current density 50, 100, 200, 400, 500 and 50 mA g^{-1} for 10 cycles each.

Results and discussion 3.

3.1 Characterization

To study the surface morphology and structure of the oxidized ceramic composites and the carbonized ceramic/carbon composite fibres, SEM images were taken at 5000 and 15,000 magnification (figure 1). It can be seen in figure 1a and b that the oxidized SnO₂ composite fibres exhibited a short cylindrical structure with particles embedded on the surface. In comparison, the SEM images of composite fibres with (1:1) (SnO₂:TiO₂) ratio (figure 1c and d) show a cvlindrical structure with interconnected embedded on the surface. At a 3:2 (SnO₂:TiO₂) ratio, the cylindrical structure was no longer present, instead a short micro-belt structure was observed, as shown in figure 1e and f. SEM images for the ceramic/carbon composite fibres are shown in figure 1g-l, respectively. It can be observed in figure 1g and h that when coating with pure SnO₂, the short-fibre morphology disappeared and, instead, spherical particles were embedded on the surface of the FPCFs. In comparison, when using the 1:1 SnO₂:TiO₂ ratio to coat the FPCFs, spherical particles embedded on the surface as well as small nanoflakes were observed. Meanwhile, when coating FPCFs with 3:2 (SnO₂:TiO₂) ratio, the spherical particles were no longer visible and instead nanoflakes were formed and deposited on the surface of the FPCFs (figure 1k and 1).

The crystal structure and thermal decomposition of the coated fibres were studied by XRD and TGA, respectively. Figure 2a shows the diffraction patterns for all the samples, including the TiO₂, SnO₂, and SnO₂/FPCFs, the SnO₂/TiO₂ (1:1)/FPCFs, and SnO₂/TiO₂ (3:2)/FPCFs. The TiO₂ diffraction pattern shows the presence of peaks (Bragg peak assignments are given in brackets) at $2\theta = 32^{\circ}$ (110), 42.2° (101), 45.8° (200), 48.3° (111), 51.8° (210), 64.3° (211), 67° (220), 74.8° (002) and 76° (310), which correspond to the diffraction pattern of rutile [63]. The SnO₂ diffraction pattern showed peaks at the following positions: $2\theta = 31^{\circ}$ (110), 39.6° (101), 44.5° (200), 45.7° (111), 61.1° (210), 64.7° (220), 73.4° (002), 77.0° (112) and 78.6° (301), which correspond to SnO₂ in the P42/mnm space group [64]. The SnO₂/PCFs diffraction pattern shows peaks at $2\theta = 35.8^{\circ}$ (200), 37.4° (101), 51.5° (220), 52.7° (211), 65.3° (301), 74.2° (112), 75.8° (400), 76.8° (321). The diffraction peaks observed in the SnO₂/PCFs sample correspond to the diffraction peaks of Sn metal and not to SnO2 [65]. The SnO₂/TiO₂ (1:1)/FPCFs and the SnO₂/TiO₂ (3:2)/FPCFs show similar diffraction patterns with peaks located at 2θ = 32.5° (110), 35.8° (200), 37.5° (101), 42.4° (101), 51.6° (220), 52.3° (210), 52.8° (211), 64.7° (211), 65.4° (301), 74.7° (002), 74.4° (112), 75.9° (400) and 76.91° (321), (310). The diffraction peaks correspond to the presence of both TiO₂ and Sn metal in the sample [63,65]. The diffraction data indicate a reduction of the Sn(IV) to Sn(0) within the fibres after carbonization. The carbothermal synthesis of Sn(0) nanoparticles from SnO₂ at temperatures around 700°C has been previously reported [66,67].

Based on the XRD results, the SnO2 was reduced to Sn the subsequent heat treatment [24,28,68,69].

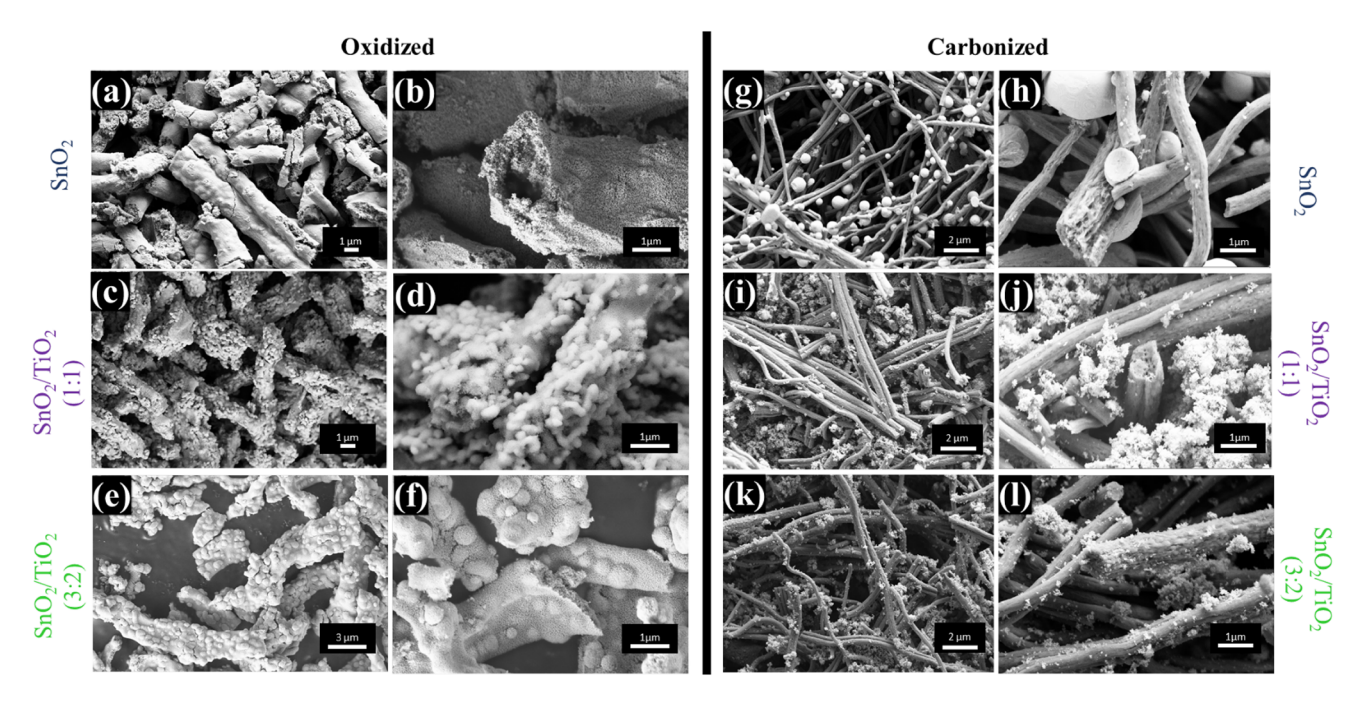


Figure 1. SEM images of (a, b) SnO₂, (c, d) (1:1) SnO₂:TiO₂, (e, f) (3:2) SnO₂:TiO₂ ceramic fibres and (g, h) SnO₂/FPCFs, (i, j) (1:1) SnO₂:TiO₂/FPCFs, (k, l) (3:2) SnO₂:TiO₂/FPCFs ceramic/carbon composite fibres at 5000× and 15,000× magnifications.

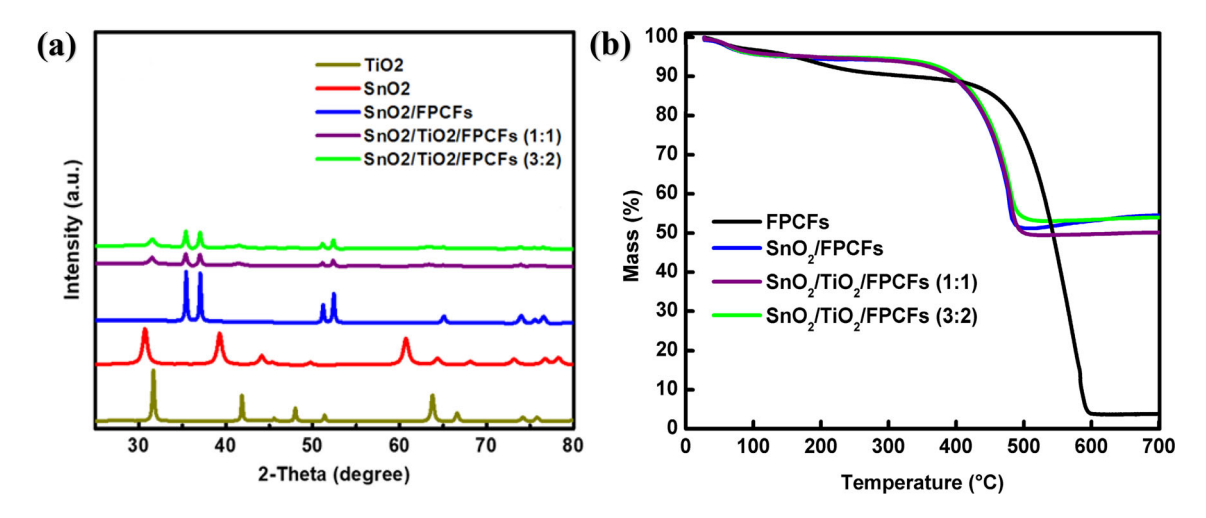


Figure 2. (a) XRD and (b) TGA of TiO₂, SnO₂, ceramic fibres and SnO₂/FPCFs, SnO₂/TiO₂ (1:1)/FPCFs and SnO₂/TiO₂ (3:2)/FPCFs ceramic/carbon composite fibres.

Furthermore, the peak at 32° in the SnO₂:TiO₂ samples can be assigned to the presence of rutile TiO_2 [70–72]. To determine the amount of active material retained within the fibres after the carbonization process, TGA experiments (figure 2b) were performed from 25 to 700°C at 5°C min⁻¹ in air. It is clear that both the uncoated and coated FPCFs exhibit two major steps (mass losses). The first loss occurs at 25-250°C for the FPCFs, at 25-180°C for the coated FPCFs, and can be attributed to the evaporation of surface bound and intercalated water in the sample. The second loss can be observed over the temperature range of 440-600°C for the FPCFs and at 380-500°C for the coated FPCFs. The residual mass of $\sim 3\%$ for the FPCFs can be attributed to the graphitized residual carbon from the PAN as well as polymer impurities. On the other hand, the residual masses of 52, 53 and 48% observed for the coated FPCFs represented the amount of SnO2 and SnO2/TiO2 and carbon present in the sample after carbonization. Based on the TGA results of the SnO₂/TiO₂/C composite anode with 3:2 SnO₂:TiO₂ ratio, the percentages of the SnO₂/TiO₂, graphitized residual carbon with polymer impurities and carbon in the composite electrode were 52, 3 and 45%, respectively. The total mass of the SnO₂/TiO₂/C composite anode was about 3.32 mg and based on the TGA results (figure 2b), the mass of the SnO₂/TiO₂ active material in the electrode was about 1.73 mg, while the mass of carbon in the electrode was about 1.49 mg. Therefore, the weight percentage of SnO₂ in the composite electrode with 3:2 ratio was 31.2% (1.04 mg out of 3.32 mg), while for the TiO₂, the weight percentage was 20.8% (0.69 mg out of 3.32 mg).

Figure 3a–d shows a high resolution TEM image with the measured d-spacing in the (3:2) SnO₂:TiO₂/FPCFs. The lattice spacing observed in the figure was consistent with the inter-planar spacing for TiO₂ (rutile) crystals. The distances between adjacent lattice planes were measured and found to have spacings of 3.25 Å, which is consistent with

the (311) d-spacings observed in the XRD results and in agreement with results reported [73,74]. However, the Sn metal nanoparticles were not observed in the TEM images. This may be due to the fibres being amorphous or the Sn nanoparticles are very small crystallites, which would result in the signal being lost in the background scattering from the larger fibres. Another explanation is that the Sn(0) nanoparticles were not homogeneously distributed across the fibres. The TEM results are consistent with those obtained by XRD on the diffraction pattern of TiO_2 (figure 2a).

Figure 4 provides EDS mappings of the (3:2) SnO₂/TiO₂/FPCF, which show uniform distribution of the C, N, O, Sn and Ti in the composite fibres. This indicates successful coating of the oxidized fibres on the PAN fibrous mat, which can result in good structure stability and improved electrochemical performance of the composite-fibre anode.

To determine the compositions and the chemical states of the components, XPS characterization analysis was conducted on the ceramic/carbon composites. The XPS survey for the SnO₂/TiO₂/FPCFs with 3:2 (SnO₂:TiO₂) ratio (figure 5) shows several peaks representing Sn, O, Ti and C. Figure 5b shows the Ti 2P_{5/2} and 2P_{3/2} regions for the composite fibres with 3:2 (SnO₂:TiO₂) ratio. The Ti 2P XPS spectrum was determined to consist of two separate peaks, which were located at 459.2 and 464.9 eV. The existence of the two peaks is indicative of Ti present in the sample as TiO_2 [75–77]. The third peak located around 472.6 eV is attributed to the presence of the Ti 2P satellite feature [76,77]. Figure 5c shows the $Sn_{5/2}$ and $Sn_{3/2}$ regions of the SnO₂/TiO₂/FPCFs sample, which was deconvoluted into four peaks. The peaks at 485.6 and 487.3 eV correspond to the presence of Sn(0) and Sn(II), which were also observed in the $3d_{3/2}$ region, with peaks located at 494.0 and 495.8 eV [78]. SnO₂ was not observed in the XRD results in figure 2a, due to a

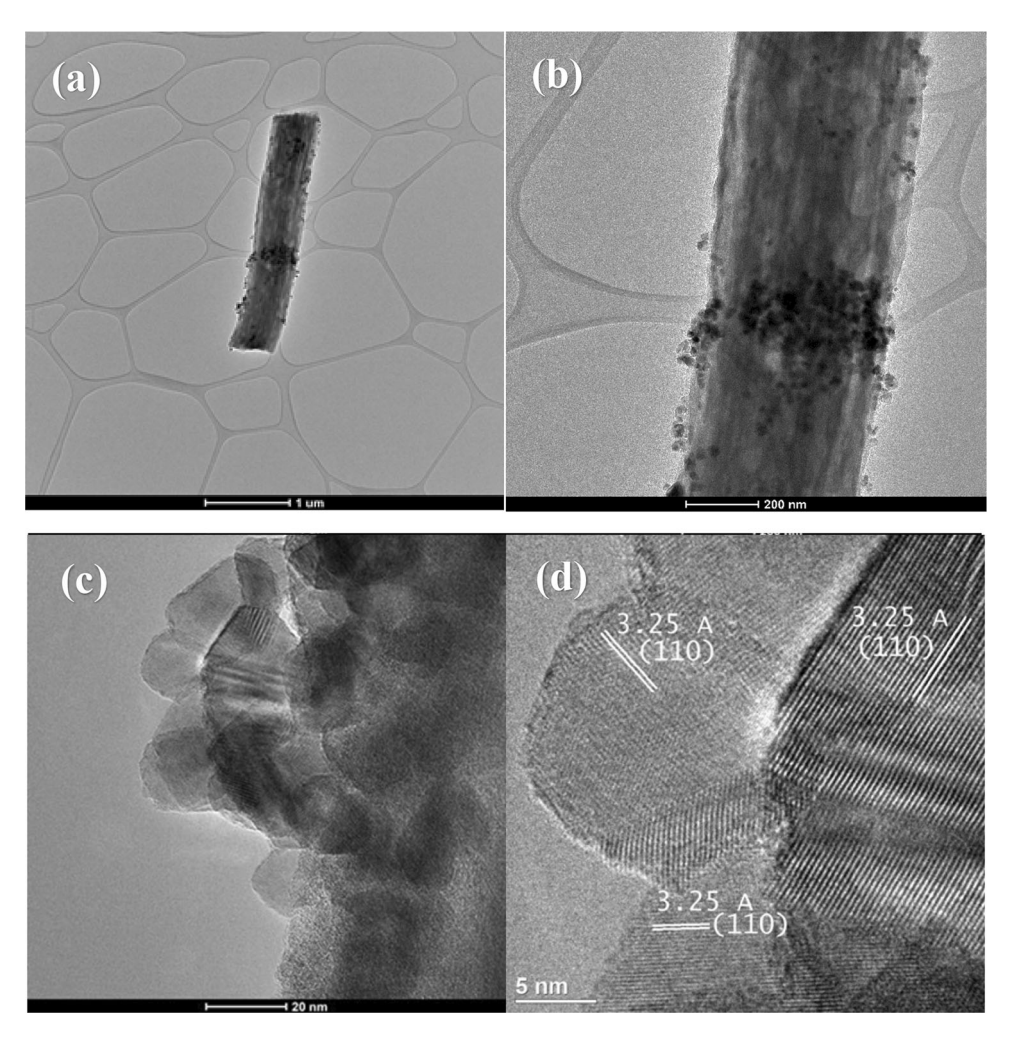


Figure 3. (a–d) High-resolution TEM images of (3:2) SnO₂/TiO₂/FPCFs.

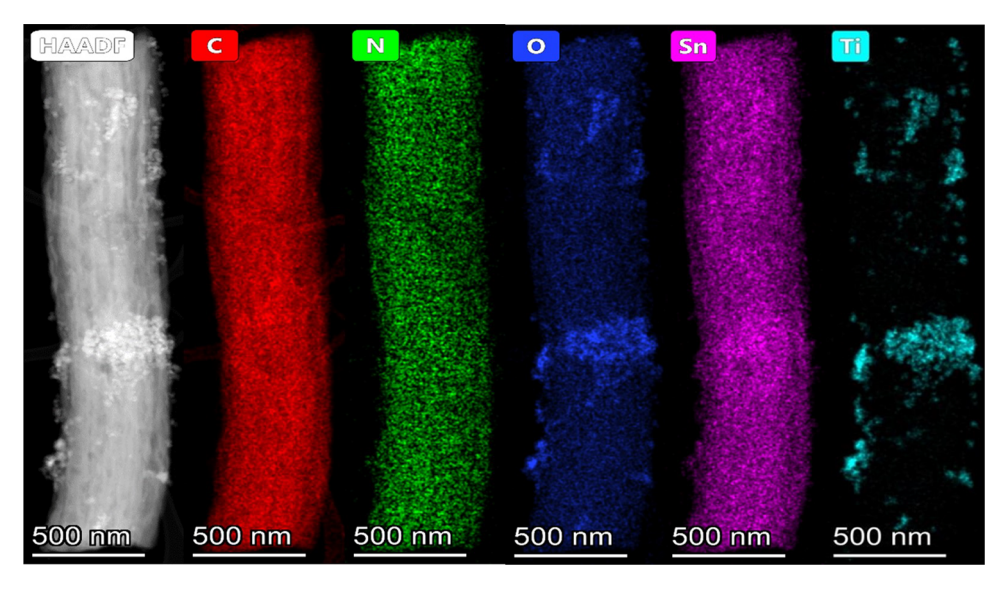


Figure 4. High-angle annular dark field image and EDS mapping for C, N, O, Sn and Ti in the (3:2) SnO₂/TiO₂/FPCFs.

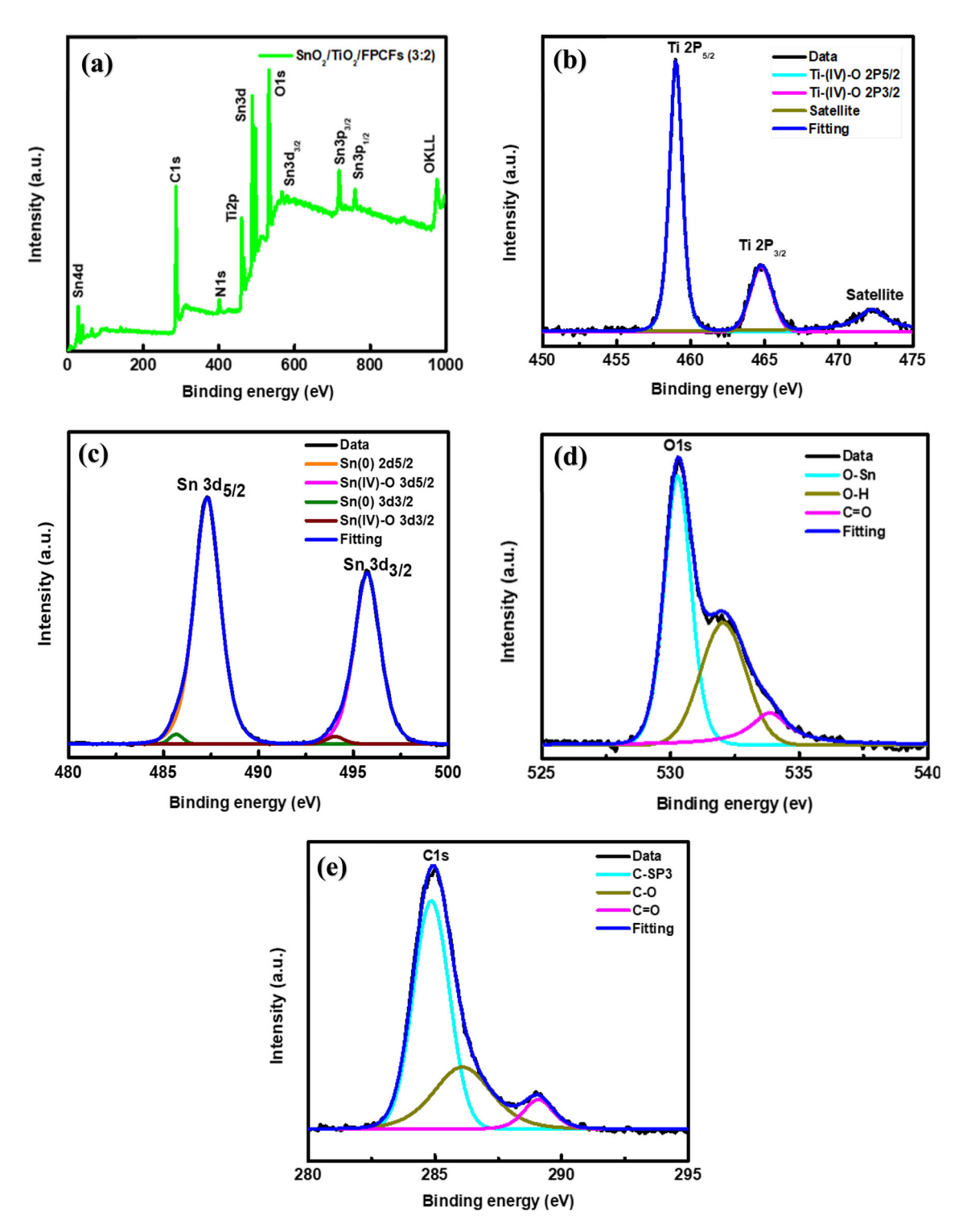


Figure 5. (a) XPS survey spectra and high-resolution spectra of (b) Ti 2p, (c) Sn3d, (d) O1s and (e) C1s of the SnO₂/TiO₂/FPCFs with 3:2 (SnO₂:TiO₂) ratio.

combination of surface layer thickness and crystallinity. The O 1S XPS data shown in figure 5d indicate that the spectrum consisted of three peaks located at 530.7, 532.1 and 533.3 eV. These three peaks are indicative of high oxidation state metal such as Ti(IV) or Sn(IV) and the

formation of C-O/C=O bonds [79–81]. C 1S spectrum is shown in figure 5e, which was deconvoluted into three peaks located at 284.7, 285.6 and 288.8 eV, indicative of the presence sp³ carbon (C-C bonds), C-O bonds and C=O bonds, respectively [79,81].

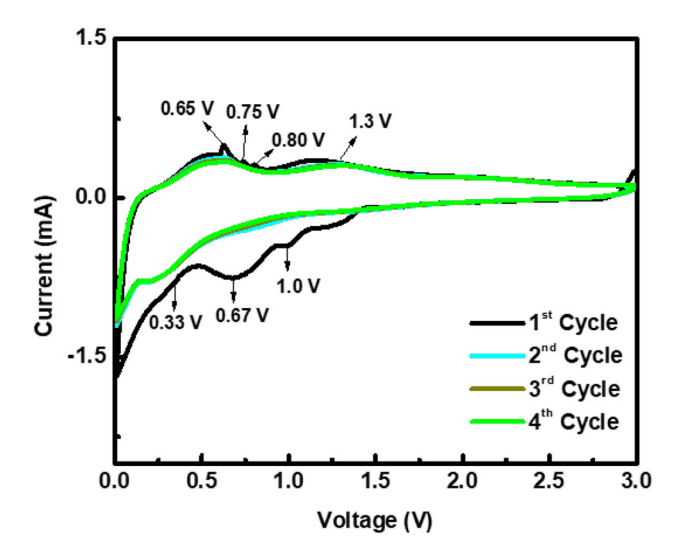


Figure 6. CV curves of the (3:2) SnO₂:TiO₂/FPCFs composite.

3.2 Electrochemical performance

To study the lithiation/delithiation reactions of the anodes, CV tests were performed for 4 cycles over a voltage potential window of 0.05-3 V and a scan rate of 0.1 mV s⁻¹. Figure 6 shows the CV curves for the (3:2) SnO₂:TiO₂/FPCFs composites, which demonstrated the best electrochemical performance when compared to the SnO₂/FPCFs and the (1:1) SnO₂:TiO₂/FPCFs. During the first cycle, three main reduction peaks are observed at 1, 0.67 and 0.33 V. These peaks represent the breakdown of electrolyte, the surface electrolyte interface formation, and the alloying reaction between Li and Sn, respectively. Additionally, the oxidation peaks at 0.62, 0.74 and 0.8 V are ascribed to the de-alloying of Li_xSn, while the broad peak at 1.2 V represents the extraction of lithium from the carbon and overlaps with the peak at 1.27 V that corresponds to the insertion/extraction of lithium from titanium [19,23,25,68,82,83]. Equation (1) represents the irreversible reaction of SnO₂ with LiO₂ to form Li_xSn, which contributes to the first irreversible capacity. Equation (2) corresponds to the reversible capacity that results from the alloying/de-alloying of Sn and Li. Equation (3) illustrates the insertion/extraction reaction between lithium and TiO2, while equation (4) represents the interaction between Li and the carbon fibres. After the first cycle, the CV curves overlap each other, indicating good capacity reversibility of the SnO₂/TiO₂/FPCFs composite anode with 3:2 (SnO₂:TiO₂) ratio.

$$SnO_2 + 4Li^+ + 4e^- \rightarrow Sn + 2Li_2O \tag{1}$$

$$Sn + xLi^{+} + xe^{-} \leftrightarrow Li_{x}Sn \ (0 \le x \le 4.4)$$

$$TiO_2 + xLi^+ + xe^- \leftrightarrow Li_xTiO_2(0 \le x \le 1)$$
 (3)

$$6C + xLi^{+} + xe^{-} \leftrightarrow Li_{x}C_{6}(0 < x < 1)$$
 (4)

It is worthwhile to note that the CV scan of the SnO₂/TiO₂/C composite-fibre electrode (figure 6) showed that the redox

peaks for TiO₂ disappeared completely. This behaviour and changes in the TiO₂ redox peaks (or anodic peak) can be due to the compact carbon layer, which can inhibit the penetration of electrolyte. The low wettability of TiO2 towards the electrolyte can also affect the intercalation/deintercalation of TiO2 with Li⁺. Similar results were reported by Zhao et al [84]. Moreover, weak redox peaks in the CV scan of SnO₂/TiO₂@CNFs with 1.5:1 SnO₂ to TiO₂ ratio were reported by Mou et al [46] while the charge/discharge profile of the SnO₂/TiO₂@CNFs anode did not reflect any plateau characteristics of TiO₂. These results support the fact that the carbon coating does indeed affect the penetration of electrolyte into the TiO₂ particles. Results reported by Jiang et al [85] on SnO₂/TiO₂@C anode also showed a wide peak at 1.89 V characteristic of a reversible reaction of TiO₂. However, the charge/discharge profile did not show any existence of voltage plateau associated with TiO₂. Similar results were also reported on SnO₂/TiO₂/graphene anode [86].

Results reported on SnO₂/TiO₂/C composite anodes showed that the charge/discharge profiles did not show obvious delithiation plateaus of anatase TiO₂ at 2.15 V, probably due to the contribution of SnO₂ and higher carbon content [36]. More work is needed to investigate the effect of carbon coating on the electrochemical performance of SnO₂/TiO₂composite fibres.

To investigate the electrochemical performance of the SnO₂/FPCFs, (1:1)SnO₂:TiO₂/FPCFs SnO₂:TiO₂/FPCFs, galvanostatic charge/discharge experiments were performed at a current density of 100 mA g⁻¹ from 0.05 to 3.0 V for 100 cycles. Figure 7a and b shows the cycling performance of the ceramic/carbon composite fibres after the 1st and 100th cycles. At the 1st cycle, the SnO₂/FPCFs, (1:1) SnO₂:TiO₂/FPCFs and (3:2) SnO₂:TiO₂/FPCFs delivered a discharge capacity of 1903, 1920 and 1839 mAh g^{-1} , respectively. Such large capacities can be attributed to the high theoretical capacity of Sn/SnO₂ as well as the large amount of Li⁺ intercalated with carbon in the carbon-fibre matrix during the first cycle. However, such high capacities are also irreversible due to the formation of the surface electrolyte interface layer that consumes a substantial amount of Li⁺. For this reason, the charge capacity ceramic/carbon composite fibres decreased to 1290, 1240 and 1197 mAh g⁻¹, respectively, resulting in low coulombic efficiencies of 67, 64 and 65% for the SnO₂/FPCFs, (1:1) SnO₂:TiO₂/FPCFs and the (3:2) SnO₂:TiO₂/FPCFs, respectively (figure 7d). However, after the second cycle, the coulombic efficiency increases to 98% for all ceramic/carbon composites and remains stable, indicating good reversibility of the carbon fibres. Figure 7c shows the electrochemical performance of SnO₂, TiO₂, FPCFs and SnO₂/TiO₂/FPCFs with different SnO₂ to TiO₂ ratios. It can be seen in the figure that the SnO₂ anode exhibits poor electrochemical performance, while FPCFs and TiO₂ electrodes delivered moderate capacity compared to that for SnO₂/TiO₂/FPCFs electrodes.

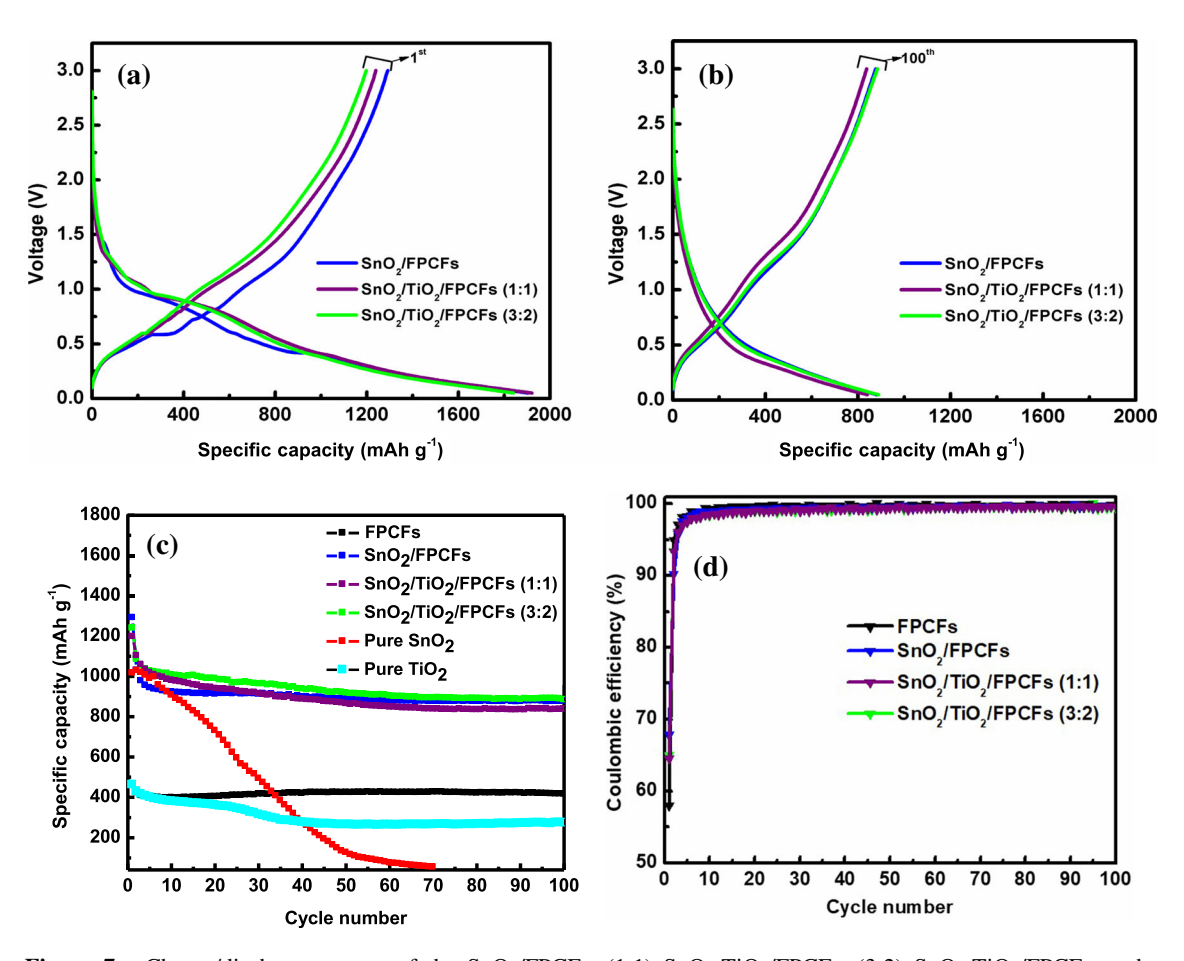


Figure 7. Charge/discharge curves of the $SnO_2/FPCFs$, (1:1) $SnO_2:TiO_2/FPCFs$, (3:2) $SnO_2:TiO_2/FPCFs$ at the (a) 1st and (b) 100th as well as the (c) charge capacity and (d) coulombic efficiency after 100 cycles at a current density of 100 mA g^{-1} .

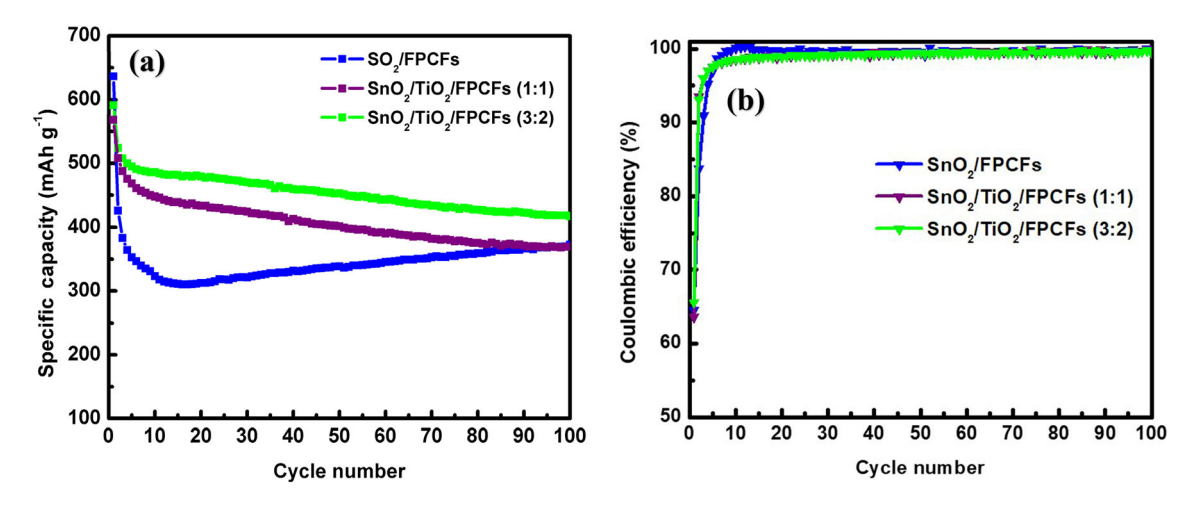


Figure 8. (a) Charge profiles and (b) coulombic efficiency of the $SnO_2/FPCFs$, (1:1) $SnO_2:TiO_2/FPCFs$ and (3:2) $SnO_2:TiO_2/FPCFs$ ceramic/carbon composite fibres after 100 cycles at a current density of 200 mA g⁻¹.

After 100 cycles, the (3:2) SnO_2 : TiO_2 /FPCFs delivered a reversible capacity of 890 mAh g⁻¹, while the SnO_2 and (1:1) SnO_2 : TiO_2 /FPCFs anodes exhibited a capacity of 877 and 840 mAh g⁻¹, respectively. As shown in figure 7c, though the capacity of the (3:2) SnO_2 : TiO_2 /FPCFs

composite was slightly higher, the overall cycling stability demonstrated by this composite was better than that of the SnO₂/FPCFs and the (1:1) SnO₂:TiO₂/FPCFs, which is due to the synergistic effect of TiO₂ achieved in this study. To discuss the effects of TiO₂ and carbon–fibre matrix on the

total capacity contribution of the $SnO_2/TiO_2/FPCFs$ electrode, the electrochemical performance of SnO_2 , TiO_2 and FPCFs anodes were evaluated (figure 7c). The main contribution of capacity comes from SnO_2 , while TiO_2 primarily stabilizes the SnO_2 anode. In fact, TiO_2 acts as a more stable material to isolate SnO_2 and has a combined effect with carbon matrix to stabilize the structure of the electrode material. Similar results were reported on the effect of TiO_2 on the electrochemical performance of SnO_2 anodes [87].

To resolve the capacity contribution from each component in the $SnO_2/TiO_2/C$ (3:2), a rough estimation was achieved in a similar manner to that reported on a similar system [87]. After 100 cycles, the FPCFs anode delivered 417 mAh g⁻¹ while the TiO_2 electrode delivered 274 mAh g⁻¹. When the

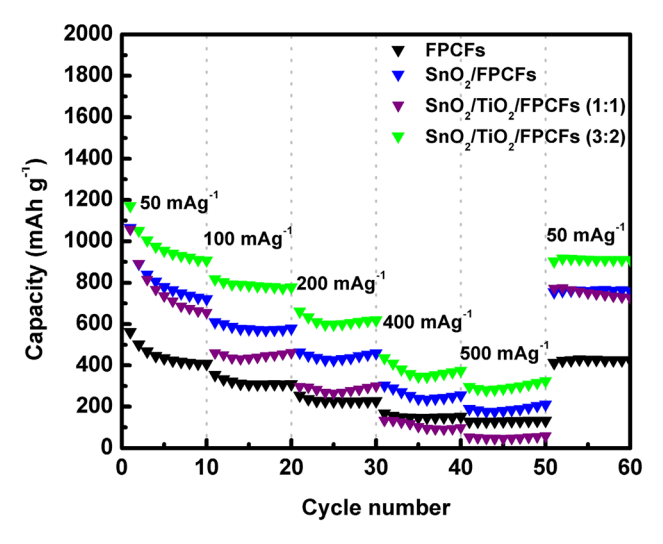


Figure 9. Rate performance of the SnO₂/FPCFs, (1:1) SnO₂:TiO₂/FPCFs and (3:2) SnO₂:TiO₂/FPCFs ceramic/carbon composite fibres at different current densities.

 SnO_2 was added, the $SnO_2/TiO_2/C$ composite fibres delivered a capacity of 890 mAh g $^{-1}$ after 100 cycles at 100 mA g $^{-1}$. It can be roughly estimated that the SnO_2 attributed 617 mAh g $^{-1}$ to the total capacity of the composite-fibre electrode considering that the content of SnO_2 and TiO_2 in the sample were 31.2 and 20.8%, respectively. Our finding is similar to that reported on SnO_2/TiO_2 nanocomposites dispersed at porous carbon (not fibres), where the contribution of SnO_2 (41.2%) to the composite electrode capacity was 813 mAh g $^{-1}$ out of 1045 mAh g $^{-1}$ [87].

To gain more insight on the cycling performance of the ceramic/carbon composites, charge/discharge cycles were also carried at 200 mA g⁻¹ for 100 cycles over a potential window of 0.05-3.0 V. As expected, it can be observed in figure 8a and b that the fibres coated with (SnO₂:TiO₂)/ FPCFs demonstrated better cycling stability when compared to SnO₂/FPCFs, due to the addition of TiO₂, which reduced the capacity loss over the first 20 cycles. At the first cycle, the SnO₂/FPCFs demonstrated a higher charge capacity of 636 mAh g⁻¹ compared to the (1:1)(SnO₂:TiO₂)/FPCFs and (3:2)(SnO₂:TiO₂)/FPCFs, which delivered charge capacities of 568 and 591 mAh g⁻¹, respectively. The lower capacity delivered by the 1:1 (SnO₂:TiO₂)/FPCFs was caused by the addition of TiO2, which hindered the overall lithium storage of the composite due to its lower theoretical capacity. However, after 100 cycles, the (3:2) (SnO₂:TiO₂)/FPCFs retained a larger capacity of 420 mAh g⁻¹, while the SnO₂ and the (1:1) (SnO₂:TiO₂)/FPCFs only yielded capacities of 369 and 370 mAh g⁻¹, respectively. The improved electrochemical performance of the (3:2) (SnO₂:TiO₂)/FPCFs can once again be attributed to TiO₂, which can mitigate the large volume expansion of SnO₂ during lithiation/delithiation, thereby improving both the capacity retention and the overall cycling stability.

To investigate the rate capability of the ceramic/carbon composites, charge/discharge experiments were performed

Table 1. Electrochemical performance comparison of SnO₂/TiO₂/PFCFs (3:2) with reported similar results on SnO₂/TiO₂/C composites.

| Materials | Current density (mA g ⁻¹) | Specific capacity (mAh g ⁻¹) | Number of cycles | References |
|--|---------------------------------------|--|------------------|------------|
| SnO ₂ /TiO ₂ @/PFCFs (3:2) | 100 | 891 | 100 | This work |
| SnO ₂ @TiO ₂ @@CNFs-1.5:1 | 100 | ~700 | 150 | [46] |
| r-TiO ₂ -NRs@r-SnO ₂ -NRs/CC | 100 | 700 | 100 | [88] |
| TiO ₂ NSs@SnO ₂ @C | 1000 | ~500 | 300 | [89] |
| SnO ₂ NC/TiO ₂ (B)NT/MWCNT | 100 | ~500 | 90 | [90] |
| SnO ₂ -TiO ₂ @-CNS | 100 | 1046 | 100 | [85] |
| SnO ₂ @TiO ₂ @@C-2 | 100 | 1045 | 100 | [87] |
| Hetero-nanostructure of SnO ₂ @TiO ₂ @@C | 200 | 676 | 50 | [39] |
| SnO ₂ @TiO ₂ @Ns@C | 200 | 642 | 450 | [35] |
| Rutile SnO ₂ @TiO ₂ @nanorods/carbon cloth | 100 | 700 | 100 | [88] |
| Hollow SnO ₂ @TiO ₂ @C nanobelts | 200 | ~804 | 500 | [91] |
| SnO ₂ /TiO ₂ //C nanospheres | 200 | 687 | 400 | [92] |

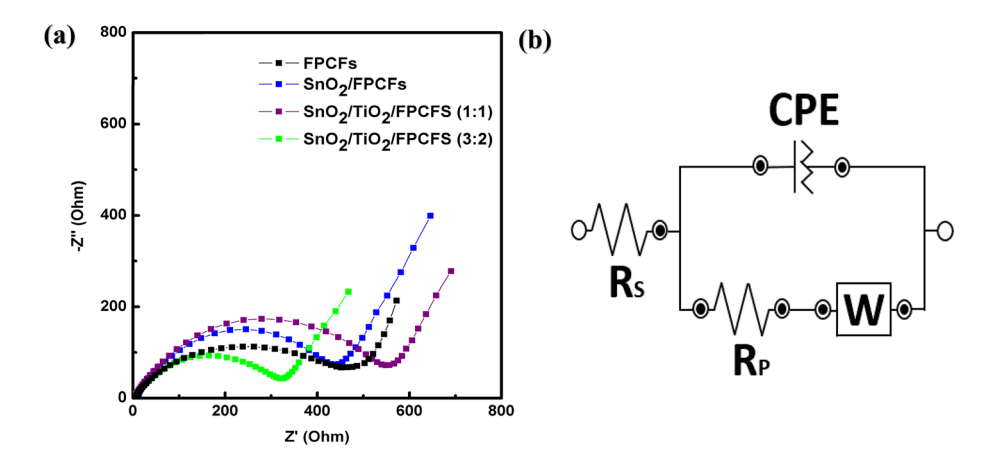


Figure 10. Nyquist plots (**a**) of the SnO₂/FPCFs, (1:1) SnO₂:TiO₂/FPCFs and (3:2) SnO₂:TiO₂/FPCFs ceramic/carbon composite fibres before cycling and (**b**) the equivalent circuit.

at 50, 100, 200, 400, 500, and back at 50 mA g⁻¹ for 10 cycles each. It can be seen in figure 9 that the fibres coated with (3:2) SnO₂:TiO₂ outperformed all the other composites. When the current density was increased to 500 mAh g⁻¹, the (3:2) (SnO₂:TiO₂)/FPCFs retained a capacity of 323 mAh g⁻¹, while the SnO₂/FPCFs and the pure FPCFs showed capacities of only 210 and 130 mAh g^{-1} , respectively. In contrast, the (1:1) (SnO₂:TiO₂)/FPCFs yielded the lowest capacity, 39 mAh g⁻¹, due to the excessive addition of TiO₂ that lowered the capacity of the overall composite. When the current density was brought back to 50 mA g⁻¹, the (3:2) (SnO₂:TiO₂)/FPCFs delivered a capacity of 908 mAh g⁻¹, while the SnO₂/FPCFs, (1:1) (SnO₂:TiO₂)/FPCFs and pristine FPCFs yielded capacities of 758, 727 and 424 mAh g⁻¹, respectively. Most importantly, the (3:2) (SnO₂:TiO₂)/FPCFs demonstrated a 100% reversibility and achieved the highest capacity compared to the SnO₂/FPCFs and the (1:1) (SnO₂:TiO₂)/FPCFs, which makes this composite a material of interest for use as an anode in LIBs.

A comparison between the electrochemical performance of the SnO₂/TiO₂/PFCFs and those reported on SnO₂/TiO₂ based anodes is summarized in table 1. The SnO₂/TiO₂/PFCFs (3:2) delivered a better capacity than most of the reported results on similar anode. However, the preparation method of the SnO₂/TiO₂/PFCFs composite anodes used in this work is different from those shown in table 1. As discussed in the Materials and Experimental sections, the SnO₂/TiO₂/PFCFs were prepared by coating the oxidized SnO₂/TiO₂/short fibres on the PAN/PMMA fibres followed by carbonization at 700°C. To the best of our knowledge, this is the first-time to report such results on coated SnO₂/TiO₂/C fibres.

To further analyse the electrochemical properties and kinetics of the as-prepared anodes, EIS measurements were performed at an open-circuit voltage over a frequency range between 0.1 and 100,000 Hz and the results are shown in figure 10. The Nyquist plots in figure 10a can be divided into

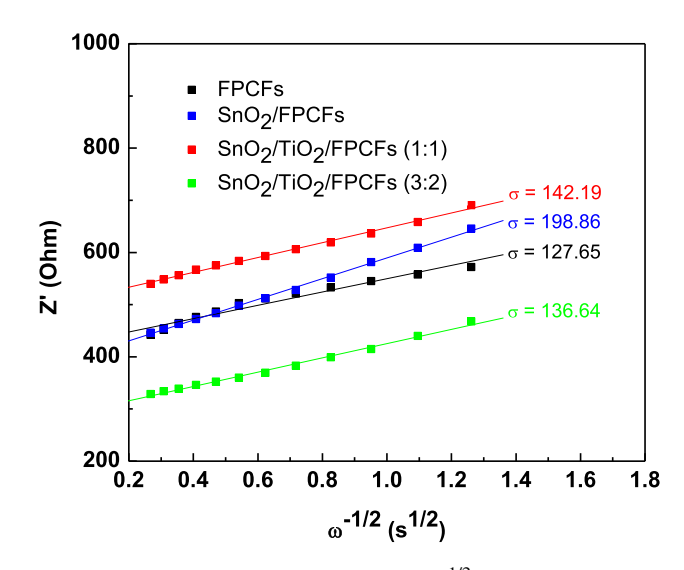


Figure 11. The fitting curves of Z'vs. $\omega^{-1/2}$ in the low frequency range of Nyquist plots.

two sections: a semicircle located at the high-medium frequencies, and a line in the low frequency range. The semicircle can be ascribed to the diffusion of Li⁺ through the surface electrolyte interface layer and the charge transfer resistance at the electrode-electrolyte interface. The line at low frequencies is assigned to the diffusion of Li⁺ through the active material. The EIS results were fitted to the equivalent circuit illustrated in figure 10b. In this circuit, R_s , R_p , W and constant phase element (CPE) represent the electrolyte solution resistance, the charge transfer resistance (polarization resistance), the Warburg impedance and the constant phase-angle element that reflects the double-layer capacitance, respectively. Based on the Nyquist plots shown in figure 10a, the FPCFs, SnO₂/FPCFs, (1:1) SnO₂:TiO₂/FPCFs and (3:2) SnO₂:TiO₂ /FPCFs demonstrated an overall resistance of 500, 430, 570 and 370 Ω , respectively. The improved resistance of the (3:2) (SnO₂:TiO₂)/FPCFs can be attributed

| Sample | | $R_{\mathrm{p}}\left(\Omega\right)$ | СРЕ | | W | |
|---|--------------------------------|-------------------------------------|-----------------------|------|----------------------------|--|
| | $R_{\rm s}\left(\Omega\right)$ | | Y _o (μMho) | n | ν Y _o (μMho) | $\sigma \ (\Omega \ \mathrm{cm^2 \ s^{-0.5}})$ |
| FPCFs | 4.8 | 422.4 | 46.2 | 0.65 | 0.005 | 127.65 |
| SnO ₂ /FPCFs | 7.81 | 405 | 29.1 | 0.73 | 0.0031 | 198.86 |
| SnO ₂ /TiO ₂ /FPCFs (1:1) | 4.1 | 522 | 29.5 | 0.7 | 0.0045 | 142.19 |
| SnO ₂ /TiO ₂ /FPCFs (3:2) | 2.09 | 301 | 33.7 | 0.68 | 0.005 | 136.64 |

Table 2. The fitting parameters of all samples used in the equivalent circuits of figure 10b.

to the synergistic effect of the SnO_2 and TiO_2 particles within the flexible carbon–fibre matrix, which resulted in improved Li^+ transport and lower charge transfer resistance when compared to the other composite electrodes [32]. The frequency values at R_s , R_P (or R_{ct}) and W were 100 kHz, ≈ 100 Hz and 0.1 Hz, respectively (figure 10a and b). The frequency range for the Warburg impedance for all anodes was between 0.1 Hz and approximately 100 Hz.

The EIS results of figure 10a were fitted using Nova software (Metrohm Autolab). The Warburg coefficient or (factor), σ , was determined by plotted Z' vs. $\omega^{-1/2}$ in the low frequency range of Nyquist plots (figure 10a). The fitting results are shown in figure 11. The Warburg coefficient, σ was determined from the slope of Z' vs. $\omega^{-1/2}$, where ω is the angular frequency [46]. Table 2 shows all the fitting parameters (R_s , R_p and W) used in the equivalent circuit as well as the Warburg coefficient σ .

As illustrated in table 2, the two parameters, Y_0 and n, were used to represent the CPE in the equivalent circuit (figure 10b), where Y_0 is the parameter containing the capacitance information while n is an empirical constant ranging from 0 to 1. When n=1, the CPE behaves as a pure capacitor, while when n=0, the CPE behaves as a pure resistor (http://www.metrohm.com/electrochemistry). For the Warburg impedance (W), Y_0 was used as a parameter containing information on the diffusion of ionic species at the interface. In fact, the Warburg impedance is characterized by having identical real and imaginary contributions, resulting in a phase angle of $+45^{\circ}$.

It is illustrated in table 2 that the SnO₂/TiO₂/FPCFs (3:2) composite-fibre anode showed higher values of σ compared to SnO₂/FPCFs and SnO₂/TiO₂/FPCFs (1:1) anodes indicating higher diffusion coefficient D, where D is proportional to $1/\sigma^2$ [46].

4. Conclusion

SnO₂ and SnO₂:TiO₂ composite fibres were successfully synthesized and coated accurately onto centrifugally spun PAN/PMMA fibrous mats, which yielded ceramic/carbon composite fibres after subsequent heat treatment. The surface morphology and structure of the as-prepared composite fibres was investigated by SEM and TEM, confirming that the

particles were successfully attached to the surface of the carbon fibres. The presence, phases and crystal structure of metallic Sn, SnO₂ as well as TiO₂ within the carbon composite fibres were confirmed by EDS, XPS and TGA, respectively. When used as a binder-free anode in Li-ion halfcells, the (3:2) (SnO₂:TiO₂)/FPCFs delivered a high reversible capacity of 890 mAh g^{-1} after 100 cycles at 100 mA g^{-1} . More interestingly, when tested at a high current density of 200 mA g⁻¹, the composite-fibre anode delivered a capacity of 419 mAh g⁻¹ after 100 cycles and coulombic efficiency of 99% after the 2nd cycle up to the 100th cycle, indicating good cyclic stability and improved performance. In rate performance tests, the (3:2) (SnO₂:TiO₂)/FPCFs initially delivered a capacity of 1171 mAh g⁻¹ at 50 mA g⁻¹ and retained a capacity of 323 mAh g^{-1} at high current rate of 500 mA g^{-1} . After the current density was lowered back to 50 mA g^{-1} , the (3:2) (SnO₂:TiO₂)/FPCFs delivered a capacity of 908 mAh g^{-1} , depicting a promising rate capability.

Acknowledgements

We acknowledge the support received from the NSF PREM program under Award DMR-2122178: UTRGV-UMN Partnership for Fostering Innovation by Bridging Excellence in Research and Student Success. This work was partially supported by the Lloyd M. Bentsen, Jr. Endowed Chair in Engineering endowment at UTRGV. The Department of Chemistry at the University of Texas Rio Grande Valley is grateful for the support provided by a Departmental Grant from the Robert A. Welch Foundation (Grant No. BX-0048). Part of this work was carried out in the College of Science and Engineering Characterization Facility, University of Minnesota, which has received capital equipment funding from the NSF through the UMN MRSEC program under Award Number DMR-2011401.

References

- [1] Chen K-H, Namkoong M J, Goel V, Yang C, Kazemiabnavi S, Mortuza S et al 2020 J. Power Sources 471 228475
- [2] Kim J, Jeghan S M N and Lee G 2020 Micropor. Mesopor. Mater. 305 110325

- [3] Roy P and Srivastava S K 2015 J. Mater. Chem. A 3 2454
- [4] Lee B-S 2020 Polymers 12 2035
- [5] Pampal E S, Stojanovska E, Simon B and Kilic A 2015 J. Power Sources 300 199
- [6] Zhang X, Ji L, Toprakci O, Liang Y and Alcoutlabi M 2011 Polym. Rev. 51 239
- [7] Goriparti S, Miele E, De Angelis F, Di Fabrizio E, Zaccaria R P, Capiglia C *et al* 2014 *J. Power Sources* **257** 421
- [8] Wang O, Mao B, Stoliarov S I and Sun J 2019 PECS 73 95
- [9] Yaroslavtsev A B and Stenina I A 2020 Surf. Innov. 1
- [10] Ji L, Meduri P, Agubra V, Xiao X and Alcoutlabi M 2016 Adv. Energy Mater. 6 1502159
- [11] Jung J-W, Lee C-L, Yu S and Kim I-D 2016 J. Mater. Chem A 4 703
- [12] Wang Q, Ping P, Zhao X, Chu G, Sun J and Chen C 2012 J. Power Sources 208 210
- [13] Akia M, Mkhoyan K A and Lozano K 2019 Mater. Sci. Eng. C 102 552
- [14] Ji L, Lin Z, Alcoutlabi M and Zhang X 2011 Energy Environ. Sci. 4 2682
- [15] Li Z, Yin Q, Hu W, Zhang J, Guo J, Chen J et al 2019 J. Mater. Sci. 54 9025
- [16] Reddy M, Subba Rao G and Chowdari B 2013 Chem. Rev. 113 5364
- [17] Li Q, Li H, Xia Q, Hu Z, Zhu Y, Yan S et al 2021 Nat. Mater. 20 76
- [18] Reddy R C K, Lin J, Chen Y, Zeng C, Lin X, Cai Y et al 2020 Coord. Chem. Rev. 420 213434
- [19] Lin Z, Liu X, Xiong X, Wei S, Liu W and Lin Z 2020 Chem. Commun. 56 10187
- [20] Luo J, Xia X, Luo Y, Guan C, Liu J, Qi X et al 2013 Adv. Energy Mater. 3 737
- [21] Sun Y-N, Goktas M, Zhao L, Adelhelm P and Han B-H 2020 J. Colloid Interface Sci. 572 122
- [22] Tian Q, Chen Y, Sui Z, Chen J and Yang L 2020 Electrochim. Acta 354 136699
- [23] Hassan F M, Chen Z, Yu A, Chen Z and Xiao X 2013 Electrochim. Acta 87 844
- [24] Liao J Y and Manthiram A 2014 Adv. Energy Mater. 4 1400403
- [25] Yang Z, Wu H H, Zheng Z, Cheng Y, Li P, Zhang Q et al 2018 Front. Chem. 6 533
- [26] Ding Y, Hu L, He D, Peng Y, Niu Y, Li Z et al 2020 Chem. Eng. J. 380 122489
- [27] Liu M, Fan H, Zhuo O, Chen J, Wu Q, Yang L et al 2020 Nano Energy 68 104368
- [28] Ryu J, Kim H, Kang J, Bark H, Park S, Lee H et al 2020 Small 16 2004861
- [29] Akurati K K, Vital A, Hany R, Bommer B, Graule T and Winterer M 2005 Int. J. Photoenergy 7 153
- [30] Aravindan V, Sundaramurthy J, Kumar E N, Kumar P S, Ling W C, von Hagen R et al 2014 Electrochim. Acta 121 109
- [31] Chen J S and Lou X W 2013 Small 9 1877
- [32] Li R, Xiao W, Miao C, Fang R, Wang Z and Zhang M 2019 Ceram. Int. 45 13530
- [33] Shi H, Zhou M, Song D, Pan X, Fu J, Zhou J et al 2014 Ceram. Int. 40 10383
- [34] Sun L, Xie J, Lei G, Liu X, Ma J and Zhang J 2021 CrystEngComm 23 2992
- [35] Bao D and Tian Q 2018 Mater. Lett. 229 48
- [36] Han M, Mu Y and Yu J 2020 Adv. Mater. 1 421

- [37] Liu M, Li X, Ming H, Adkins J, Zhao X, Su L et al 2013 New J. Chem. 37 2096
- [38] Lu Y, Yanilmaz M, Chen C, Dirican M, Ge Y, Zhu J et al 2015 ChemElectroChem 2 1947
- [39] Tian Q, Xu H, Li L and Bao D 2017 Mater. Lett. 209 197
- [40] Agubra V A, De la Garza D, Gallegos L and Alcoutlabi M 2016 J. Appl. Polym. Sci. 133 42847
- [41] Mao X, Hatton T A and Rutledge G C 2013 Curr. Org. Chem. 17 1390
- [42] Zuniga L, AgubraV, Flores D, Campos H, Villareal J and Alcoutlabi M 2016 J. Alloys Compd. 686 733
- [43] Cai M, Yuan D, Zhang X, Pu Y, Liu X, He H et al 2020 J. Power Sources 461 228123
- [44] Li X, Chen W, Qian Q, Huang H, Chen Y, Wang Z et al 2021 Adv. Energy Mater. 11 2000845
- [45] Zaarour B. Zhu L and Jin X 2020 ChemistrySelect 5 1335
- [46] Mou H Y, Chen S X, Xiao W, Miao C, Li R, Xu G L et al 2021 Ceram. Int. 47 19945
- [47] Li T Y, Chen Y, Wang L F and Xia X 2020 J. Solid State Electr. 24 781
- [48] Fang D, Li L, Xu W, Li G, Luo Z, Zhou Y et al 2014 Mater. Res. Express 1 025012
- [49] Javed K, Oolo M, Savest N and Krumme A 2019 Crit. Rev. Solid State Mater. Sci. 44 427
- [50] Ji H, Ma C, Ding J, Yang J, Yang G, Chao Y et al 2019 J. Power Sources 413 42
- [51] Sarkar K, Gomez C, Zambrano S, Ramirez M, de Hoyos E, Vasquez H et al 2010 Mater. Today 13 12
- [52] Lv R, Zhu Y, Liu H, Na B, Huang Y and Xie X 2017 J. Appl. Polym. Sci. 134 44515
- [53] Padilla-Gainza V, Morales G, Rodríguez-Tobías H and Lozano K 2019 J. Appl. Polym. Sci. 136 47643
- [54] Chavez R O, Lodge T P and Alcoutlabi M 2021 Mater. Sci. Eng. B 266 115024
- [55] Chavez R O, Lodge T P, Huitron J, Chipara M and Alcoutlabi M 2021 J. Appl. Polym. Sci. 138 50396
- [56] Jia H, Dirican M, Zhu J, Chen C, Yan C, Zhu P et al 2018 J. Alloys Compd. 752 296
- [57] Agubra V A, Zuniga L, De la Garza D, Gallegos L, Pokhrel M and Alcoutlabi M 2016 Solid State Ion 286 72
- [58] Atıcı B, Ünlü C H and Yanilmaz M 2021 Polym. Rev. 62 1
- [59] Valdez A 2018 Forcespinning of metal oxides and metal sulfides and their applications as alternative anode materials for lithium-ion and sodium-ion batteries (The University of Texas Rio Grande Valley)
- [60] Akia M, Salinas N, Luna S, Medina E, Valdez A, Lopez J et al 2019 J. Mater. Sci. 54 13479
- [61] Lu Y, Fu K, Zhu J, Chen C, Yanilmaz M, Dirican M et al 2016 J. Mater. Sci. 51 4549
- [62] Kim D, Lee D, Kim J and Moon J 2012 ACS Appl. Mater. Interfaces 4 5408
- [63] Meagher E and Lager G A J T C M 1979 Can. Mineral. 17 77
- [64] Baur W H 1956 Acta Cryst. 9 515
- [65] Wyckoff R W G 1963 Cryst. Struct. 1 7
- [66] Lian P C, Wang J Y, Cai D D, Liu G X, Wang Y Y and Wang H H 2014 J. Alloys Compd. 604 188
- [67] Wang J, Li D L, Fan X Y, Gou L, Wang J J, Li Y et al 2012 J. Alloys Compd. 516 33
- [68] Wang D, Li X, Yang J, Wang J, Geng D, Li R et al 2013 Phys. Chem. Chem. Phys. 15 3535
- [69] Wei Z, Mao H, Huang T and Yu A 2013 J. Power Sources 223 50

- [70] Kaplan R, Erjavec B, Dražić G, Grdadolnik J and Pintar A 2016 Appl. Catal. B: Environ. 181 465
- [71] Su C. Hong B-Y and Tseng C-M 2004 Catal, Today 96 119
- [72] Wu J-M, Shih H C and Wu W-T 2005 Nanotechnology 17 105
- [73] Chalastara K, Guo F Q, Elouatik S and Demopoulos G P 2020 Catalysts 10 407
- [74] Du Y E, Li J, Liu Y F, Niu X J, Gu F and Feng Q 2016 RSC Adv. 6 9717
- [75] Erdem B, Hunsicker R A, Simmons G W, Sudol E D, Dimonie V L and El-Aasser M S 2001 Langmuir 17 2664
- [76] Pal B, Bakr Z H, Krishnan S G, Yusoff M M and Jose R J 2018 Mater. Lett. 2225 117
- [77] Södergren S, Siegbahn H, Rensmo H, Lindström H, Hagfeldt A and Lindquist S-E 1997 J. Phys. Chem. B 101 3087
- [78] Babu B, Reddy I N, Yoo K, Kim D and Shim J 2018 Mater. Lett. 221 211
- [79] Kwan Y C G, Ng G M and Huan C H A J 2015 Thin Solid Films 590 40
- [80] Kwoka M and Krzywiecki M J 2017 Beilstein J. Nanotechnol. 8 514
- [81] Stathi P, Gournis D, Deligiannakis Y and Rudolf P J L 2015 Langmuir 31 10508

- [82] Xu Y, Liu Q, Zhu Y, Liu Y, Langrock A, Zachariah M R et al 2013 Nano Lett. 13 470
- [83] Zou L, Gan L, Lv R, Wang M, Huang Z H, Kang F et al 2011 Carbon 49 89
- [84] Zhao W, Yuan Y, Du P, Zhu M, Yin S and Guo S 2021 ChemElectroChem 8 3282
- [85] Jiang W, Xiong D, Wu S, Gao J, Wu K, Li W et al 2022 Ceram. Int. 48 27174
- [86] Wei B, Yan S, Jia D, Feng C, Yin J and Wang Z 2022 Inorg. Chem. Commun. 145 110048
- [87] Shi X, Liu S, Tang B, Lin X, Li A, Chen X et al 2017 Chem. Eng. 330 453
- [88] Liu Q, Wang L, Zhao K, Yan W, Liu M, Wei D et al 2020 Electrochim. Acta 354 136727
- [89] Wang J, Wang J, Song X, Qi S and Zhao M 2020 Appl. Surf. Sci. 511 145625
- [90] Zheng J, Ma D, Wu X, Dou P, Cao Z, Wang C et al 2017 J. Mater. Sci. 52 3016
- [91] Tian Q, Li L, Chen J, Yang L and Hirano S 2018 J. Power Sources **376** 1
- [92] Tian Q, Mao Y, Zhang X and Yang L 2018 Appl. Surf. Sci. **447** 408